Marine Chemistry 140–141 (2012) 24–32

Contents lists available at SciVerse ScienceDirect

Marine Chemistry

journal homepage: www.elsevier.com/locate/marchem

Metallic nanoparticle enrichment at low temperature, shallow CO_2 seeps in Southern Italy

Enikö Kadar [a,*], Andrew Fisher [b], Björn Stolpe [c], Roy M. Harrison [c,e], Francesco Parello [d], Jamie Lead [c]

[a] Plymouth Marine Laboratory, Prospect Place, The Hoe, Plymouth PL1 3DH, UK
[b] School of Geography, Earth and Environmental Sciences, University of Plymouth, Drake Circus, Plymouth PL4 8AA, UK
[c] School of Geography, Earth and Environmental Sciences, University of Birmingham B15 2TT, UK
[d] Department of Earth and Marine Sciences, University of Palermo, 90123 Palermo, Italy
[e] Department of Environmental Sciences/Center of Excellence in Environmental Studies, King Abdulaziz University, Jeddah 21589, Saudi Arabia

ARTICLE INFO

Article history:
Received 28 May 2012
Received in revised form 3 July 2012
Accepted 3 July 2012
Available online 16 July 2012

Keywords:
Nanoparticles
Hydrothermal seeps
Iron

ABSTRACT

We report on metal enrichment along a natural pH gradient owing to increased CO_2 degassing at cold, shallow seeps of Vulcano Island in the Mediterranean Sea, off Sicily. We assessed composition of unfiltered and filtered seawater (<100 nm) along acidic zones ranging between ambient and pH 5, and showed that most seep derived elements are present as nanoclusters which then aggregate into larger colloids while mixing with ambient seawater along a pH gradient. Size and elemental composition of such naturally occurring nanoparticles assessed by modern characterisation methods were in good agreement with the results from conventional analytical methods.

We provide analytical evidence for the presence in the water column of a large fraction of seep derived elements (e.g. approximately 50% of iron, over 80% of Mn, 100% of Cr, S and Zn) in the form of nano sized particles (e.g. <100 nm) even at typical open ocean pHs. We launch in situ sampling protocols and sample preparation procedures for multi-method suitable to obtain accurate measurements on nanoparticles from environmental samples. Based on our results a first insight to the formation of natural nanoparticles at cold CO_2 seeps is presented and the persistence of such nano-clusters in the surrounding seawater is stipulated.

1. Introduction

Deep sea hydrothermal vents are considered "chemical reactors" for the formation of both organic and inorganic compounds and their transformation through abiotic and biotic processes (Luther, 2004), and are a significant source of metals to the ocean. Steep pH gradients combined with metal enriched fluid emissions typical at these high temperature deep sea hydrothermal vents (Kadar et al., 2005) are conditions known to facilitate the formation of Fe-rich nanoparticles (NPs) (Kennedy et al., 2004; Kim et al., 2008; Yucel et al., 2011; Wu et al., 2011). Recent research suggests that an unknown fraction of this flux escapes from precipitation/flocculation reactions partly due to stabilisation by organic ligands (Sander and Koschinsky, 2011; Toner et al., 2009; Bennett et al., 2008), and due to nanoparticles reported to be kinetically stable (Yucel et al., 2011).

Contrasting such high temperature dominated system emissions from the shallow, high temperature vents (cold seeps) have metal concentration several orders of magnitude lower (Kim et al., 2008). Formation of metallic nanoclusters may therefore be less likely to occur in cold seeps, but cannot be ruled out and has not been adequately investigated to date. Nanoparticle formation under the reducing conditions typical at cold seeps is a result of mobilisation of metals due to CO_2 seepage in the sediment owing to dissolution of particles and release of adsorbed metals on the surface of the solids, and also due to changes of decomposition rates of biogenic particulate material due to decreased pH and pE (Ardelan et al., 2009). The significance of the contribution of such metallic nanoclusters to the biogeochemical cycling of Fe at shallow underwater CO_2 emissions is unknown and needs to be addressed.

Whilst sampling challenges in extreme environments (Kadar and Powell, 2006) and the lack of analytical techniques for detection and characterisation of natural NPs (Lead et al., 2000) have prevented in depth study of the actual morphology, mineralogy and chemical properties of the NPs emitted in deep sea hydrothermal fluids until recently, shallow seeps may be a more accessible site for such studies. The contrasting geological settings, distributions, biogeochemistry, and dynamics of vent and seep ecosystems render distinctive characteristics ranging from the source of reduced compounds available for microbial transformation into energy through chemical oxidation, to the nature of the substratum. It is fair to assume therefore that the

* Corresponding author. Tel.: +44 1752 633450(direct); fax: +44 1752 633101.
E-mail address: enik@pml.ac.uk (E. Kadar).
URL: http://www.pml.ac.uk (E. Kadar).

0304-4203/$ – see front matter © 2012 Elsevier B.V. All rights reserved.
doi:10.1016/j.marchem.2012.07.001

environmental fate of NPs within the shallow, cold, sunlit settings of CO_2 seeps will be quite different from deep-sea vents, which warrants our comparative discussion.

The shallow fumaroles within the geothermal field in Southern Italy have recently been in the spotlight (Spencer-Hall et al., 2008) providing natural laboratory conditions to study physiological adaptations to ocean acidification i.e. valuable predictors of future ocean ecology owing to their elevated CO_2 flux. The geothermal field from the Levante Bay comprises both terrestrial and submarine gas emissions emerging a few metres from the beach at about 1 metre depth. The resulting gas emissions from the hydrothermal aquifer are associated with magmatic fluids coming from the crater fumaroles and modified by low-temperature subsurface processes (Chiodini et al., 1995). The gas emissions are characterised by high CO_2 contents > 90% volume and a significant variability of H_2S ranging from 0.8 to 2.5% volume (Capaccioni et al., 2001). The large variability of H_2S in the gas discharge can be attributed to the interaction between metal sulphides and hydrothermally altered volcanic and weakly acid waters. Thermal water discharges from the Istmo-Porto di Levante beach further complicate the water chemistry of the bay (Aiuppa et al., 2000) by their input of elevated conductivity, high Na and Cl content, very low pH and Eh and high content of volatile metals, due to acid gas condensation (Aiuppa et al., 2000). Such underwater volcanic emissions create a natural pH gradient that provide excellent sites to study the environmental behaviour (i.e. stability, mobility, and persistence) of metal-rich and organic NPs from various volcanic fluids and/or gas. Taking advantage of the geochemically distinct, shallow fumaroles as natural sites of NP emission it is uniquely possible to study transport and fate of NPs under natural environmental conditions, investigate their tendency to aggregate and interact with other particles under different bio-geo-chemical settings. Understanding their environmental fate and behaviour may help us distinguish such naturally present NPs from engineered NPs, a fundamental nanoscience challenge.

In an effort to better understand environmental fate and behaviour of natural NP we report on the prevalent types of metal-rich natural NPs along a natural pH gradients created by submarine volcanic gas emissions at a geochemically distinct geothermal system in Vulcano Island in South Italy. Our aim is to conduct an integrated study of these hydrothermal NPs to reveal their composition, size distribution, surface topology and chemical reactivity. Specific aims were to characterise these NPs along a pH gradient determined by distinct CO_2 fluxes and investigate the relationships between NP structure and the geochemical settings at hydrothermal seeps. In addition, we provide key information on methods suitable for detection of naturally present NPs.

2. Materials and methods

2.1. Water sampling for multi-element analysis using ICP-MS and ICP-OES

Triplicate seawater samples were collected at four sites (Fig. 1) along a natural pH gradient at the sub aquatic volcanic emissions in Levante Bay on the island of Vulcano (Southern Italy 38°25′N; 14°57′E) including: site A with visible gas emission as small bubbles and an average pH ~7 (low enough to cause physiological stress to calcifying organisms); site B at a distance of 40 m away from A along the shore with no visible gas emissions; and the off-shore control site C with pH ~8, 150 m away and separated from the venting source by a geographical barrier. The extreme acidic site D was also investigated as the place with constant, very intense CO_2 emission, a consequent average pH 5 and lack of inhabitant macro-organisms. Water samples were collected and stored in 500 mL, acid washed HDPE flasks. Triplicate samples were taken manually by

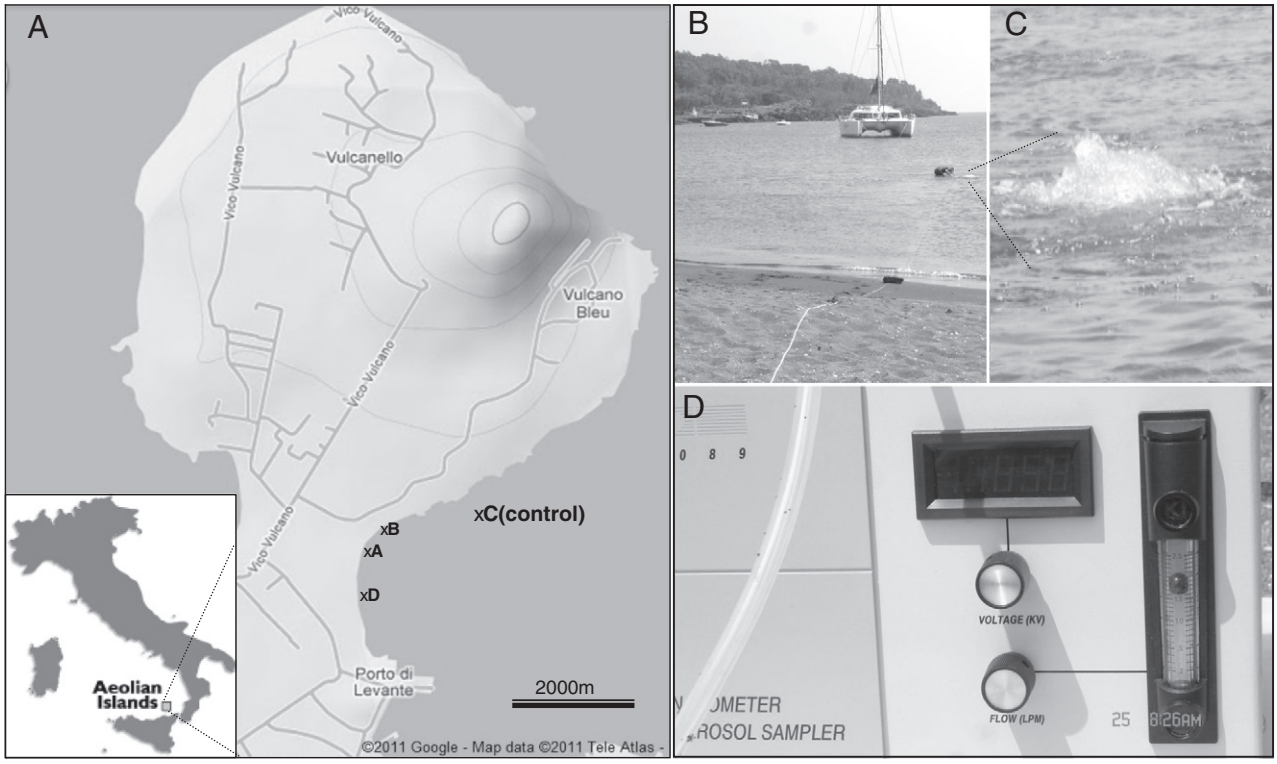

Fig. 1. The sites of sampling along a natural pH gradient at the sub aquatic volcanic CO_2 emissions off the island of Vulcano (Southern Italy 38°25′N; 14°57′E) as follows: site A, with conspicuous gas emission and pH ~7.6 that is known to cause physiological stress to calcifying organisms and thus it is referred as "low pH site"; site B with no visible gas emission and pH ~7.9 referred as "mid pH"; site C (control) was chosen circa 150 m from the venting sources with ambient sea water pH of 8.1; and site D with constantly very intense CO_2 emission, average pH 5 and a consequent lack of inhabitant macro-organisms.

opening the narrow necked flasks at about 50 cm below the water surface in order to avoid sampling any surface films (Morley et al., 1997) and to allow CO_2 dissolution through the water column. Simultaneously snapshot values of physico-chemical parameters were recorded (Table 1) using a hand held multi-parameter water quality meter (WTW). Three sub samples of all samples (three replicates from each site) were filtered in situ on 100 nm pore size polycarbonate membranes (Millipore) and the filtrates were acidified to pH 2 by addition of 10 μL mL^{-1} of ultrapure, concentrated HNO_3 until analysis for elemental composition using ICP-MS and/or ICP-OES. The macro elements were analysed using a Varian 725-ES ICP-OES instrument with the following operating conditions: forward power = 1.4 kW; coolant gas flow = 15 L min^{-1}; auxiliary gas flow = 1.5 L min^{-1}; nebuliser gas flow = 0.68 L min^{-1}; viewing height = 8 mm; replicate read time = 4 s; nebuliser type: v-groove; spray chamber type = Sturman–Masters.

Trace-elements were analysed using a Thermo Scientific X Series 2 ICP-MS instrument. Operating conditions were: power = 1.4 kW; coolant gas flow = 13 L min^{-1}; auxiliary gas flow = 0.7 L min^{-1}; nebuliser gas flow = 0.80 L min^{-1}; dwell time = 10 ms; sweeps = 50; nebuliser type = concentric glass; spray chamber type = PC^3; collision cell gas = 7% hydrogen in helium at a flow rate of 3.5 mL min^{-1}.

The samples were diluted by a factor of 10 (with 2% nitric acid) to overcome problems with salt clogging the injector of the ICP torch or the sampler and skimmer cones. Matrix-matched standards were prepared using a 10-fold dilution of the certified reference material NASS 5 (National Research Council Canada). Internal standards of 10 μg L^{-1} In and Ir were also used for the ICP-MS analyses to compensate for any temporal instrumental drift. Detection limits for various elements were as follows (in nM): Cr ≤ 7; Mn ≤ 17; Co ≤ 8; Ni ≤ 15; Cu ≤ 7; Zn ≤ 12; Mo ≤ 2; Ag ≤ 3; Cd ≤ 10; Ba ≤ 6; Pb ≤ 0.5 and Fe ≤ 3.

2.2. NP characterisation

Particle size distribution, shape, micro-morphology and surface topology were studied by both transmission electron microscopy (TEM) and atomic force microscopy (AFM). TEM samples were prepared by depositing the unfiltered seawater samples on Formvar/carbon coated 300 mesh Cu grids (S162-3, AGAR Scientific); the grids were precisely covered with sample. Particles were allowed to adsorb to the carbon coating for 30 min (without drying), followed by gently immersing the grids in ultra pure water to remove un-adsorbed particles, salt and other components, and air-drying under protective cover. This methodology prevented aggregation effects due to air-drying and increased salt formation, but it is recognised that the ultrahigh vacuum TEM conditions may have altered fragile organic structures. However, our recent data (manuscript in prep.) shows that air-drying has little or no effect on images or sizing compared with imaging of samples in water. At least ten micrographs were acquired on randomly selected grids taken from various locations of the grids, ensuring representativity and statistical rigour. Electron micrographs were taken using a TEM at 80 keV (JEOL 1200EX), and particle size and shape parameters were evaluated using image analysis computer software (Digital Micrograph, Gatan Inc.). High-resolution micrographs and major element-composition of selected particle-types were thereafter acquired on a TEM operating at 200 keV (Philips Tecnai F20) equipped with energy-dispersive X-ray diffraction (EDX, Oxford Isis). AFM samples were prepared by covering freshly cleaved mica with the unfiltered seawater samples (10–20 μL), allowing particles to adsorb to the mica for 5 min, followed by gentle immersion in ultra pure water and air-drying. AFM images (XE-100, Park Systems) of 30 × 30 μm and 2 × 2 μm were obtained in air by non-contact mode at 0.5 Hz scan rate using a silicon cantilever with 42 N m^{-1} force constant and 330 kHz resonance frequency (PPP-NCHR, Nanosensors). Average particle diameters were determined by measuring the heights over the mica surface of a large number of particles (> 200 for most of the samples) using analytical computer software (XEI, Park Systems). Due to the typically skewed nature of particle distributions we report median particle heights together with upper and lower quartile values.

2.3. Sampling of hydrothermal gas

Detection of natural NPs in the hydrothermal gas from shallow CO_2 seeps was conducted for the first time using a TSI Nanometer aerosol sampler (Model 3089 NAS) that electro-precipitates NPs directly onto TEM grids and/or AFM substrates (Willeke and Baron, 1993). This instrument collects positively charged particles in the range of 2 to 100 nm using the electrostatic precipitation method by an electrode with a negative potential of up to 10,000 V. The sampler was run on a fixed flow rate (1.7 $Lmin^{-1}$) and voltage (−9.6 V) and the electric field between the grounded chamber and the electrode focuses particles onto the substrate (TEM grids and/or mica sheets for AFM), which can then be removed for analysis. The gas was captured using a plastic funnel (50 cm diameter) secured over a gas escape with a strong and constant flow (Fig. 1B and C), which was connected to the Nanometer aerosol sampler by 30 m long PVC tube (Fig. 1D).

3. Results

3.1. Total and filterable fraction of major and microelements in the water column

The physicochemical parameters captured by our discrete measurements (Table 1) do not point to distinct pH-zones within our study sites in the Levante Bay (Fig. 1) possibly owing to mixing determined by local hydro graphic conditions, morpho-dynamic parameters and site geometry. Seawater at the sampling sites A, B and C was enriched in Mn, Fe, Cr, Cu, and Zn (Table 2). In addition, Pb and Ba were only enriched in the extreme acidic site (D). Comparison between un-filtered and 0.1 μm filtered seawater concentrations showed that most elements that were enriched relative to control seawater were predominantly present as NPs, organic and/or inorganic complexes of free ions in the <100 nm fraction, with the exception of Fe, Pb, Ag and Cu. For Fe, the percentages found in the <100 nm fraction were relatively low at site A (15%), B (30%) and C (50%) indicating that Fe was mostly associated with larger (>100 nm) colloids or particles in these waters with pH 7–8 with low or no gas emission. However, the filter-passing fraction of Fe was much larger (80%) at site D with pH 5 and intense gas emission. Contrary to Fe, Pb was 100% in the filter passing fraction at sites A and B but only 35% at site D (Table 2B).

Table 1
Typical parameters including depth, pH, temperature, conductivity, O saturation and redox potential at the four sampling sites along the pH gradient. Values are seasonal single measurements taken using a portable multimeter sensor (WTW) during 2011.

Site	Depth (cm)	pH	T (°C)	Conductivity (μS cm^{-1})	O saturation (%)	Redox potential
D (extreme acidic)	150	5.91 ± 0.60	20.15	96.63	93	−171
A (low pH)	150	7.38 ± 0.55	19.76	96.03	114	−91
B (mid pH)	270	7.76 ± 0.25	19.54	95.75	119	−34
C (control Med. Sea)	250	8.03 ± 0.02	19.47	95.43	112	−52

Table 2
A.) Metal concentrations of the four sites along a pH gradient following the acid digestion and analysis using ICP-MS or ICP-OES analysis. Values are averages ± SEM, N = 3.B.) Nano-sized fraction of the volcanic elements that enrich seawater represented as % of the total concentrations detected in unfiltered samples.

A) Total conc. (mM) macro elements	D (pH 5.9)	A (pH 7.4)	B (pH 7.8)	C (control, pH 8.1)
Ca	11.14 ± 0.00	11.44 ± 0.01	11.26 ± 0.11	11.26 ± 0.13
K	10.87 ± 0.18	8.15 ± 0.54	9.24 ± 0.11	11.66 ± 0.33
Mg	53.18 ± 0.22	53.68 ± 0.10	53.31 ± 0.27	53.66 ± 0.65
Na	525.82 ± 2.71	555.70 ± 6.98	539.45 ± 7.33	538.01 ± 7.29
Sr	0.09 ± 0.00	0.09 ± 0.00	0.09 ± 0.00	0.09 ± 0.00
B	0.48 ± 0.00	0.48 ± 0.00	0.48 ± 0.00	0.48 ± 0.00
S	31.15 ± 0.33	32.28 ± 0.23	31.82 ± 0.40	31.1 ± 0.26
micro elements (nM)				
Cr[a]	5.63 ± 0.92	18.85 ± 2.35	34.07 ± 1.28	7.39 ± 1.44
Mn[a]	377.75 ± 18.64	155.13 ± 24.22	94.94 ± 16.86	48.83 ± 2.38
Fe[a]	750.18 ± 75.92	926.22 ± 63.58	479.23 ± 38.18	317.34 ± 20.03
Cu[a]	11.06 ± 6.34	n.d.	n.d.	n.d.
Zn[a]	1936.37 ± 19.15	2092.38 ± 111.99	2003.65 ± 25.56	2249.92 ± 112.13
Mo[a]	19.43 ± 1.05	39.06 ± 3.71	32.96 ± 0.59	35.05 ± 2.08
Ag[a]	n.d.	n.d.	n.d.	n.d.
Ba[a]	27.61 ± 4.91	18.87 ± 4.02	15.97 ± 4.96	25.08 ± 5.42
Pb[a]	3.61 ± 1.73	0.81 ± 0.03	1.09 ± 0.03	1.68 ± 0.19

B) % 0.1μ-filtered fraction	D (pH 5.9)	A (pH 7.4)	B (pH 7.8)	C (control, pH 8.1)
Cr	100	55.8	100	100
K	100	98	95	93
S	100	98	100	100
Mn	100	100	93	85
Fe	80	14	29	50
Zn	100	99	100	100
Pb	52	20	80	100
Cu	38	62	64	44

[a] Elements whose concentrations are significantly different from those detected in the control seawater samples.

3.2. Typical (nano) particle clusters along the natural pH gradient

The TEM micrographs of the unfiltered seawater showed the presence of particles ranging in size from a few nm to several hundred nm (Fig. 2 and Supplementary information Fig. S1). The EDX-spectra can typically give semi-quantitative information about element composition when the element makes more than about 0.1–1.0% of the total mass of specific particles on the selected area of the TEM micrographs (Utsunomiya and Ewing, 2003); Cu, C and O however, are always present in high concentrations due to background from the carbon coated Cu-grids. Micrographs from site A (Fig. 2Aa–d and Supplementary information Fig. S1 Aa–j) showed a type of large ($600 \pm {}^{1000}/_{500}$ nm, median circular diameter $\pm {}^{\text{upper quartile}}/_{\text{lower quartile}}$) electron-dense colloids with porous and entangled structure, often surrounded by smaller (a few nm) spherical particles (Fig. 2A). Similar colloids were observed on micrographs from site B (Fig. 2Ba–b and Supplementary information Fig. S1 Ba–e), although smaller in size ($200 \pm {}^{260}/_{50}$ nm). For a majority of the large colloids, at both sites A and B, EDX-spectra from the electron-dense centres of the colloids showed high signals of Fe, while S, Cl and Ca were also present albeit showing lower signals (Fig. 2Aa–b with related EDX spectra). This result strongly indicates that the colloids were largely composed of Fe-rich material, although the presence of organic matter cannot be ruled out due to the limitations in the preparation method and background presence of carbon. Some of the colloids imaged by TEM contained fibrillar and less electron-dense structures (Fig. 2Ad), suggesting that they indeed contained organic biopolymer fibrils (Perret et al., 2000; Wilkinson et al., 1997). The small, spherical and, less electron-dense particles surrounding the large colloids (Fig. 2Ab) only showed low levels of S and Ca above the background. It is possible that these particles represented organic macromolecules such as humic substances (Wilkinson et al., 1999). Interestingly, high levels of Cr were ubiquitously detected in all Fe rich colloids from site B (Fig. 2Ba,b), but not at the other sites, which was in good agreement with the ICP-MS results showing Cr concentrations in site B more than 4 times higher than in control seawater at site C (Table 2). Other types of large colloids were also present at sites A and B (Supplementary information, Fig. S1) having a more compact structure and being dominated by Ca, indicating that they may represent Ca-carbonate particles. The TEM micrographs and EDX-spectra from the control site C also showed large ($600 \pm {}^{1080}/_{480}$ nm) electron-dense Fe-rich colloids (Fig. 2Ca–c and Supplementary information Fig. S1 Ca–e), but with a different structure, e.g. composed of elongated particles or crystals. It is possible that this structural difference represented a more advanced state of Fe oxyhydroxide crystallisation, or an input of different types of organic matter from phytoplankton. In addition, different types of colloids were observed at the control site C containing high levels of sulphur, but un-detectable levels of Fe (Fig. 2Cb and Supplementary information Fig. S1 Cd, e). At site D, most of the colloids appear to be composed of smaller NPs rich in S (Fig. 2Da). In addition, a different type of particulate material was found, with high concentrations of Fe, P and Mg, and lower levels of Cr, S, Cl and Ca (Fig. 2Da–b).

The AFM-images showed large numbers of NPs in the 0.5–20 nm size range and a few larger aggregates that appeared to be composed of similar small NPs (Fig. 3 and Supplementary information Fig. S2). The diameter (height) distributions determined from AFM micrographs were not normally distributed, but followed a power law, which is typical for particles from natural waters (Mavrocordatos et al., 2007) and was $4 \pm {}^{6.6}/_{2.4}$ nm (n = 226) at site A, $3 \pm {}^{6.1}/_{1.9}$ nm (n = 201) at site B, $6 \pm {}^{9.1}/_{4.2}$ nm (n = 231) at site C and $4 \pm {}^{5.5}/_{2.5}$ nm (n = 209) at site D (median values $\pm {}^{\text{upper quartile}}/_{\text{lower quartile}}$). Statistical comparison (two-tailed Mann–Whitney *U*-test with 0.05 significance level) showed that the particle diameters were significantly different between all the samples, except for between sites A and D. It should be noted that AFM images do not reveal the composition of the particles, and that they could include organic macromolecules, which are typically prevalent in the 0.5–20 nm size range (Stolpe and Hassellöv, 2010). Although small NPs were much more

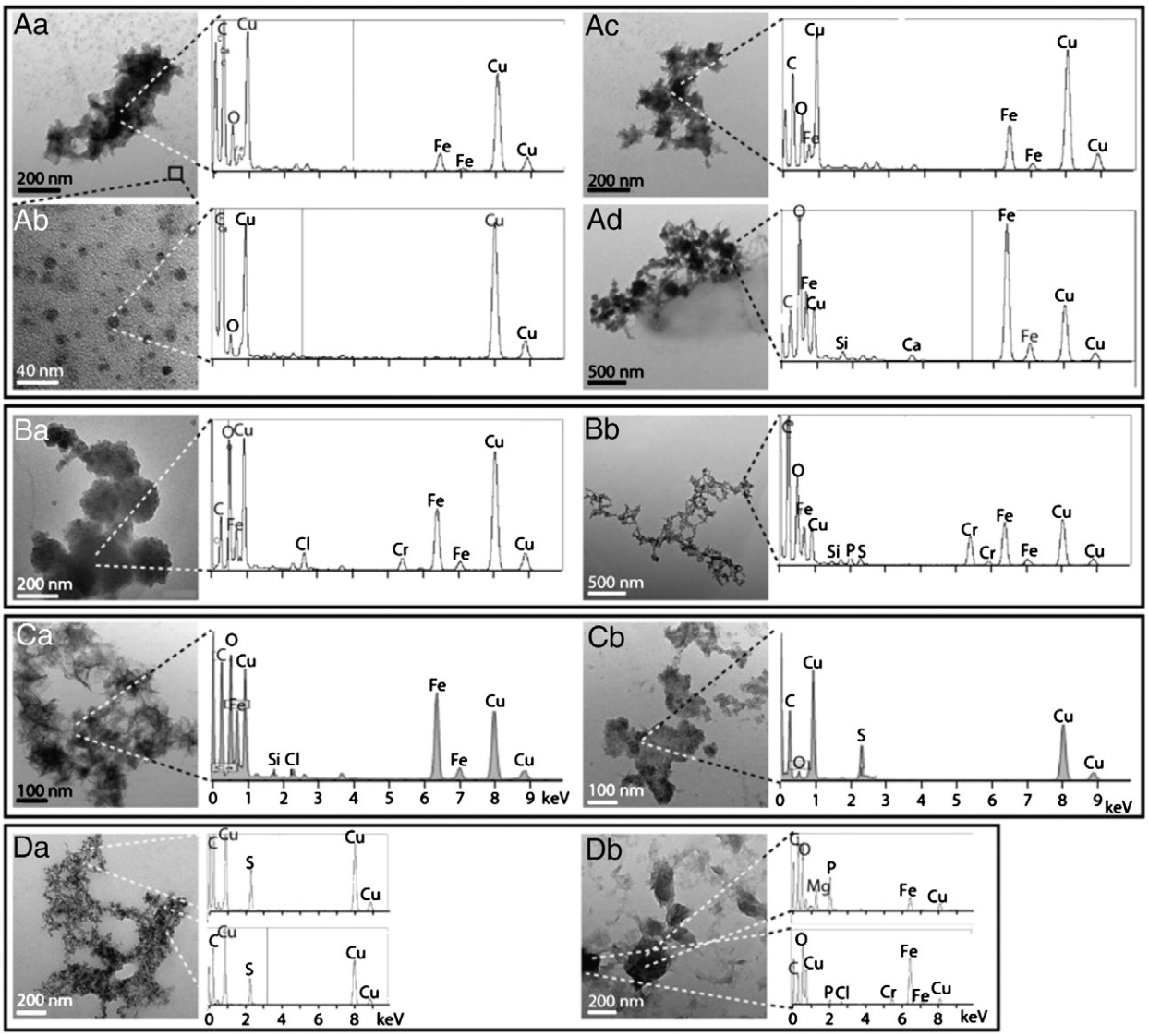

Fig. 2. Selected TEM microcraphs and related EDX spectra acquired at specific locations on the typical particles encountered in the seawater samples at the 4 sites along the pH gradients of the volcanic CO_2vents of Vulcano Island off Sicily: A (a–d) the low pH site; B (a–b) the mid pH site; C (a–b) the control site 150 m from the low pH site and D (a–b) the extremely low pH site with intense CO_2 degassing.

numerous than larger aggregates, the aggregates may represent a higher portion of the total particle mass, and may thus contain a larger proportion of Fe in the samples. If all particles are assumed to be spherical, the median particle volumes were $50 \pm {}^{150}/_{7}$ nm^3 at site A, $20 \pm {}^{120}/_{3}$ nm^3 at site B, $110 \pm {}^{400}/_{40}$ nm^3 at site C and $20 \pm {}^{90}/_{9}$ nm^3 at site D (median values and interquartile ranges). This result follows the same trend as the percentages of Fe as measured by ICPMS in the retentates of 100 nm filtration, which decreased in the order site A > site B > control > site D (Table 2B).

A range of size and shape parameters were evaluated on the Fe-rich colloids shown on the TEM and AFM-micrographs (Supplementary information, Table S1amd S3). The sphericity and solidity of the colloids (see Supplementary information for definitions) determined from TEM-micrographs were similar at the three sites, implying that no significant difference in colloid shape or porosity between the sites could be shown. In addition, the fractal dimensions of the colloids determined using a simplified approach described by Lee and Kramer (2004) (Supplementary information, Table S1), were in the range 1.77–1.86 at all four sites, indicating that they had been formed by diffusion-limited aggregation, e.g., without any strong repulsion between the smaller components forming the colloids (Lin et al., 1998). No significant difference could be shown between TEM and AFM fractal dimensions at sites B and C, but there was a small but significant difference at site A, and a highly significant difference at site D (Mann–Whitney *U*-test with $P = 0.05$ significance level). The differences could be interpreted as a change in aggregate structures in the TEM-samples as a result of drying in the ultra high vacuum inside the TEM.

3.3. Typical (nano) particles in hydrothermal gas

The use of TSI Nanometer Aerosol Sampler to capture hydrothermal gas was a pioneering success in delivering a representative gas sample from a subaquatic degassing, with sufficient mass and/or particle number, directly onto TEM and SEM/AFM grids that allowed determination of the shape morphology and chemical composition of typical positively charged particles. TEM micrographs and related EDX spectra of the hydrothermal gas showed particles in a size range from few nm to several hundred nm that were rich in S, Ca, K, Mg, P and Si with traces of Fe and Co (Fig. 4A and B). The AFM images from the same samples however, showed a low number of spherical

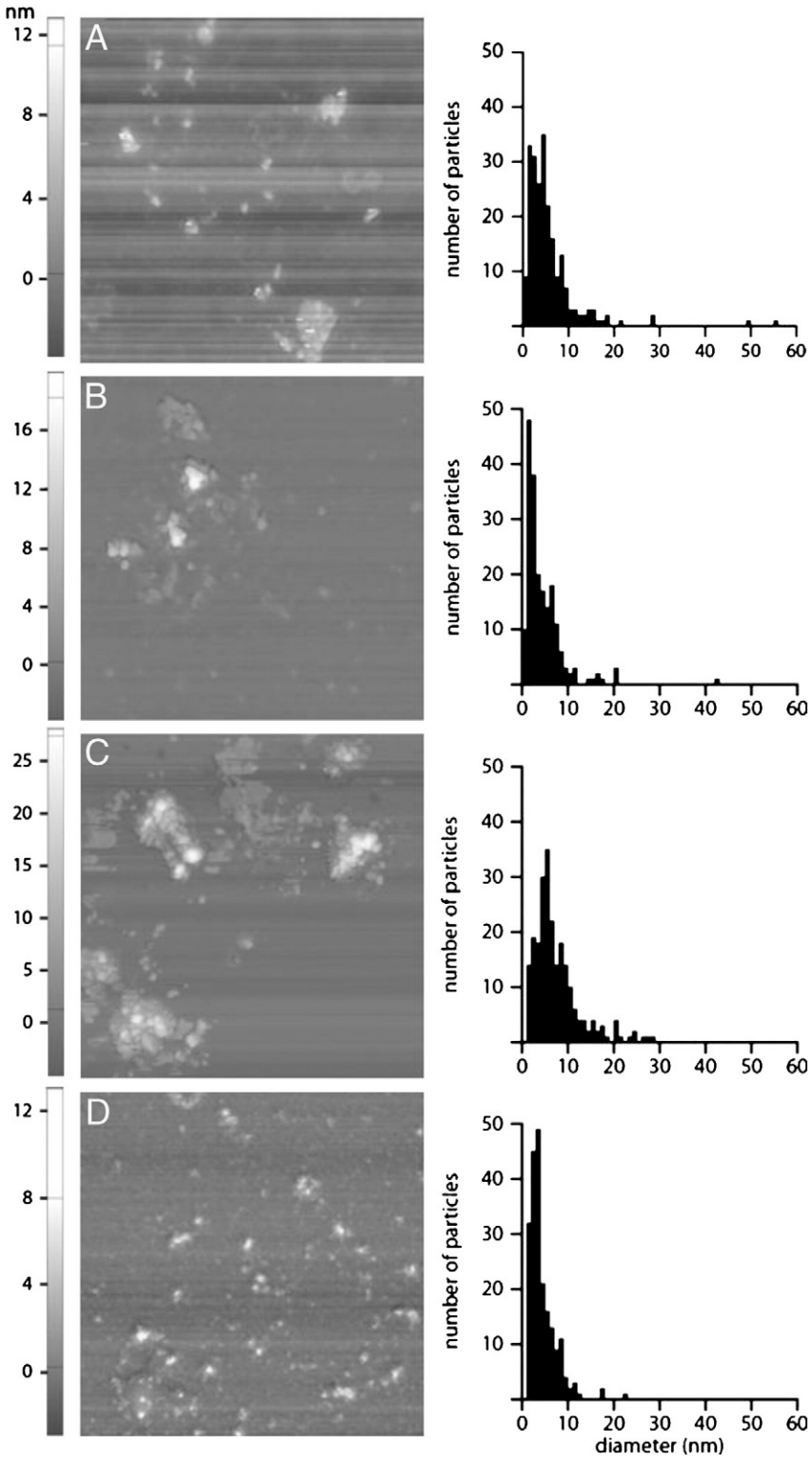

Fig. 3. Selected AFM images from the seawater samples from A) the low pH site B) the mid pH site C) the control site; D) the extremely low-pH site with intense CO_2 degassing. Histograms are showing the particle diameter distribution based on height measurements of minimum 200 particles on at least 4 different AFM images.

NPs (Fig. 4C) with a narrow size distribution of $7 \pm {}^{8.1}/_{6.5}$ nm (n = 34) (Fig. 4D).

4. Discussion

Total Fe concentrations in both unfiltered and filtered water samples (<100 nm) from the cold CO_2 seeps in Vulcano (Southern Italy) were about an order of magnitude higher than reported for other near-shore oligotrophic Mediterranean waters (Özturk et al., 2003; Sarthou and Jeandel, 2001; Morley et al., 1997), strongly indicating that this type of cold, shallow CO_2 seeps can supply significant iron input to the sea. At such high concentrations (e.g. in the order of μM), Fe in seawater is usually found predominantly associated with large particles that are retained by 0.45 μm filters (Benoit et al., 1994; Stolpe and Hassellöv, 2010). Therefore, the fact that as much as 80% of Fe at site D passed through a 100 nm filter indicates that

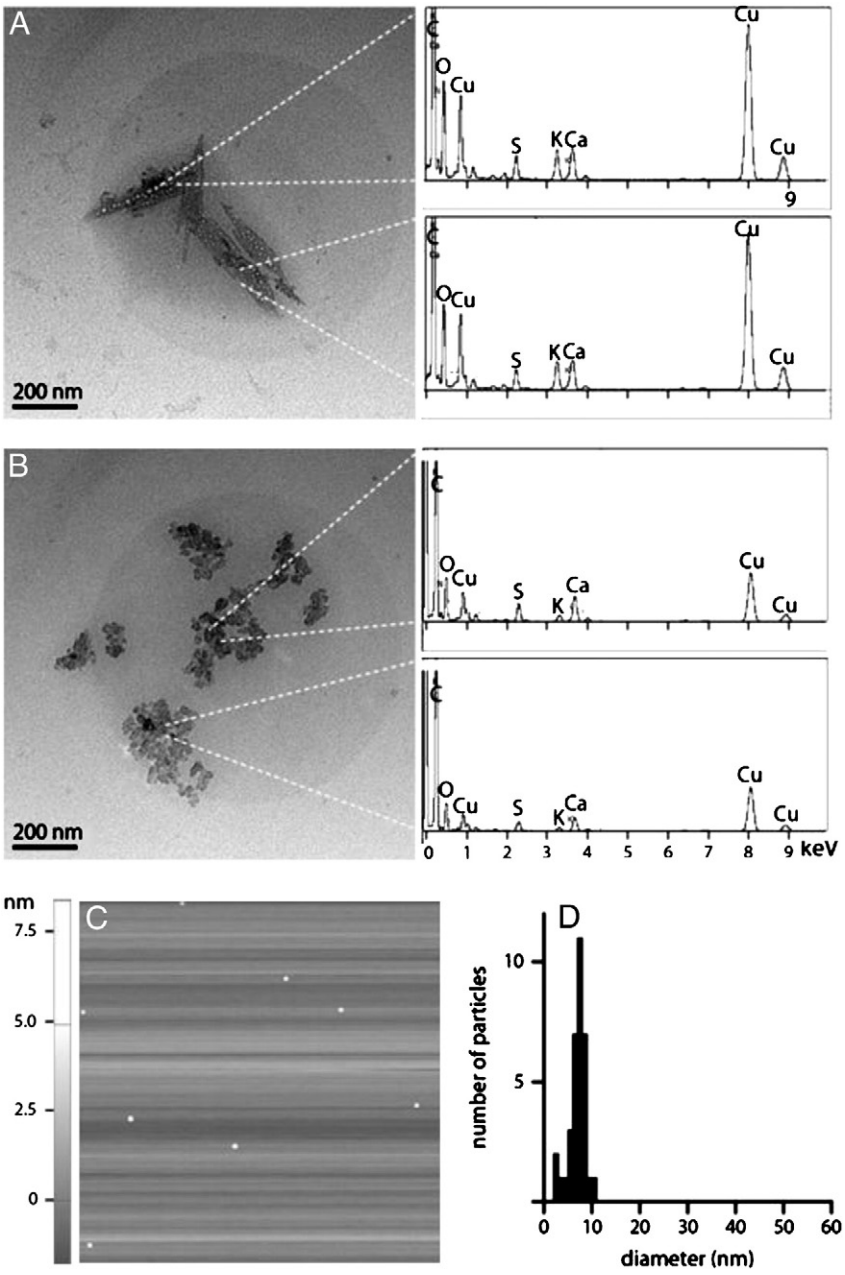

Fig. 4. Particle micromorphology, composition and size distribution in the hydrothermal gas captured using the aerosol nanoparticle sampler (low flow settings: 1.7 $Lmin^{-1}$ for 30 min and −9.6 V); A and B: selected TEM micrographs and related EDX spectra acquired at specific locations on the micrographs and C: selected AFM image and histogram showing the particle diameter distribution based on height measurements of 34 particles at 4 different AFM images. Note that regardless of their distinct morphometry typical particles captured have very similar elemental composition.

the physicochemical fractionation of Fe near these fumaroles was highly different from other near-shore marine waters. Binding of Fe to small organic complexes can explain a higher solubility than expected for inorganic suspension alone (Sander and Koschinsky, 2011; Toner et al., 2009; Bennett et al., 2008; Kuma et al., 1996), where <100 nm fractions of iron were lower (Table 2B). However, although no DOC data are available for our sample sites, the concentrations of organic matter at site D, where the <100 nm fraction of iron was the highest, is not expected to be higher than at site B and the control site, where <100 nm fractions of iron were lower (Table 2B). Therefore, the formation of iron-rich NPs around the CO_2 seeps, e.g., in the form of Fe (III) hydroxide or oxy-hydroxide and iron sulphides, may be a more likely explanation to the large percentage of <100 nm Fe found at site D. The results from TEM and AFM confirmed that NPs were prevalent in the seawater samples, but also showed that they aggregated to become larger colloids. However, the fact that Fe was comparatively high in concentration even at the control site 150 m from the seeps, and that as much as 50% of Fe there was in the <100 nm filter-passing fraction may imply similar trends to findings on Fe-rich NPs from deep sea hydrothermal vents transported to considerable distances in seawater (Yucel et al., 2011; Wu et al., 2011). Another cold seep/deep sea fumarole similarity may be the rapid aggregation and settling of some of the Fe-rich NP particles within the immediate vicinity of the fumaroles (Kuma et al., 1996; Wilkinson et al., 1997), which could explain our results on the lower <100 nm Fe fraction at site A, and the increase of this fraction from site A to the sites B and C (Table 2b). In addition, site A, which has both the highest Fe-concentration with the lowest percentage of <100 nm iron, and the

largest fraction of NPs in the >10 nm size range as shown by AFM, may receive iron from an additional source, e.g., benthic re-suspension. Similar sediment suspension may happen in the other sites to a lesser degree depending on seepage intensity and related biogeochemical processes.

The distribution of trace elements between un-filtered and 100 nm filtered samples at the different sampling stations can be explained by their inorganic speciation, organic complexation and binding to Fe-rich NPs and colloids. The large percentages of Mn and Zn in the 100 nm filtrates are in accord with their inorganic speciation being dominated by free divalent ions or chloride complexes, forming only weak complexes with organic ligands and Fe-oxyhydroxide surfaces (Long and Angino, 1977; Byrne, 2002). Cu on the other hand forms strong organic complexes (Croot, 2003) and is most likely influenced by the distribution of organic matter between un-filtered and 100 nm filtered fractions. The inorganic speciation of Pb changes from Pb-chloride complexes being dominant at lower pH, to Pb-carbonates dominating at neutral and higher pH (Long and Angino, 1977). If Pb-chloride is more readily available to adsorb to Fe-oxyhydroxide surfaces, it could explain why 77% of the Pb was associated with >100 nm particles at site D with pH 5, while 'truly dissolved' Pb-carbonate complexes could account for the large (79–100%)<100 nm Pb-fractions at the other sites with pH>7.5 (Table 2B). Ag forms strong sulphide complexes (Dyrssen, 1988) and association with the S-rich NPs at site D, and aggregation of these NPs into larger colloids at site A, could explain the Ag partitioning between filter fractions at these sites with hydrothermal activity. Mo tends to be depleted in reduced Fe–S-rich waters. The similar metal enrichment pattern of our study sites with those detected in the terrestrial thermal ground waters from near Levante Bay (in the Isthmo de Levante beach, which is characterised in detail by Aiuppa et al., 2000) indicates that these elements may have a common origin with those in the thermal aquifer. However, in depth volcanology discussions on the origin of the CO_2 seeps are beyond the scope of this work.

Generally, concentrations of inorganic aqueous species reported here are in good agreement with data from previous published data on the fumaroles in Vulcano (Amend et al., 2003). The ICP-OES analysis even failed to detect any significant difference in total dissolved sulphur concentration among study sites (possibly owing to the masking effect of the high SO_4^{2+}concentrations naturally present in seawater) despite our clear evidence that S is a chief component of the CO_2 degassing captured by the electrostatic-precipitator on the TEM grids (EDX spectra of all nano-clusters from the hydrothermal gas shown in Fig. 2). It is likely that the acid volatile fraction of sulphur accounted for most of the site specific differences, and this form is not captured by TDS using ICP-OES on acid digested seawater samples. However, S peaks were ubiquitous in EDX-spectra of all colloids in suspension at all four study sites, including control samples (Fig. 2A–D). Usually S co-occurred with Fe except for the extreme acidic site D, where two distinctive colloids were observed: the more abundant and homogenous aggregates of NPs (<10 nm) with high S content (Figs. 2Da and 3D) and the larger micron-size particles with heterogeneous composition with high Fe and P peaks that co-occur with other metallic elements with hydrothermal origin (Amend et al., 2003) such as Cr, Mg, Si, Al, Zn and Mn (Fig. 2). This may indicate that complexation of dissolved free S is fast and the resulting metal-sulphide nano-clusters appear to be consistent feature of these CO_2-degassing sites providing continuous, kinetically stable metal input to the sea, same as previously reported at deep sea hydrothermal vents (Yucel et al., 2011). However, further, in depth sulphide speciation measurements are needed for a complete understanding of metal sulphide formation at cold seeps.

Our study demonstrates the great advantages of complementing analytical chemistry with high resolution analytical TEM and AFM. This is best illustrated with the example of Cr for which chemical analysis showed distinctively high concentration in the mid pH site as compared to the other 3 sites, and which is supported by the ubiquitous Cr peaks in most X-ray spectra obtained on nano-particle clusters here. While TEM alone would have suggested the exclusive presence of macro-sized Cr-rich particles in suspension, the concentrations of Cr measured in the filtered fractions and also the AFM profiles indicate that Cr-bearing particles from site B are mostly nano-sized. It is possible that agglomeration of NPs into the large clusters shown in Fig. 2B, is due to the high vacuum during TEM analysis, while AFM, which operates under atmospheric pressure, detected a larger proportion of discrete NPs. Best size distribution and characterization of NPs, in particular those from natural environmental samples, are therefore achieved using complementary data from multiple analytical methods.

To sum up, (i) we provide a first insight to the formation of natural NPs at cold CO_2 seeps (ii) showing an enrichment in trace metals (e.g. Fe>Mn, Cr>Pb>Cu>Ba) as compared to control samples with pH 8; (iii) most of these elements are in the <100 nm fraction as indicated by both high resolution microscopy and analytical chemistry methods and (iv) the persistence of such nano-clusters in the surrounding seawater is stipulated.

Acknowledgements

Sampling and field work was financed by travel grant to EK via the Mediterranean Sea Acidification in a changing climate (MedSeA, EC FP7) project. The Natural Environment Research Council (NERC) funded facility FENAC at the University of Birmingham is acknowledged for their help with microscopy analysis (FENAC/2011/05/007 funding to EK).

Appendix A. Supplementary data

Supplementary data to this article can be found online at http://dx.doi.org/10.1016/j.marchem.2012.07.001.

References

Aiuppa, A., Dongarra, G., Capasso, G., 2000. Trace elements in the thermal ground waters of Vulcano Island (Sicily). J. Volcanol. Geotherm. Res. 98, 189–207.
Amend, J.P., Rogers, K.L., Shock, E.L., Gurieri, S., Inbuaggiato, S., 2003. Energetics of chemolithoautotrophy in the hydrothermal system of Vulcano Island, southern Italy. Geobiology 1, 37–58.
Ardelan, M.V., Steinnes, E., Lierhagen, S., Linde, S.O., 2009. Effects of experimental CO_2 leakage on solubility and transport of seven trace metals in seawater and sediment. Sci. Total Environ. 407, 6255–6266.
Bennett, S.A., Achterberg, E.P., Connelly, D.P., Statham, P.J., Fones, G.R., German, C.R., 2008. The distribution and stabilisation of dissolved Fe in deep-sea hydrothermal plumes. Earth Planet. Sci. Lett. 270, 157–167.
Benoit, G., Oktaymarshall, S.D., Cantu, A., Hood, E.M., Coleman, C.H., Corapcioglu, M.O., Santschi, P.H., 1994. Partitioning of Cu, Pb, Ag, Zn, Fe, Al, and Mn between filter-retained particles, colloids, and solution in 6 Texas estuaries. Mar. Chem. 45, 307–336.
Byrne, R.H., 2002. Inorganic speciation of dissolved elements in seawater: the influence of pH on concentration ratios. Geochem. Trans. 3, 11–16.
Capaccioni, B., Tassi, F., Vaselli, O., 2001. Organic and inorganic geochemistry of low temperature gas discharges at the Baia di Levante beach, Vulcano Island, Italy. J. Volcanol. Geotherm. Res. 108, 173–185.
Chiodini, G., Cioni, R., Marini, L., Panichi, C., 1995. Origin of the fumarolic fluids of Vulcano Island, Italy and implications for volcanic surveillance. Bull. Volcanol. 57, 99–110.
Croot, P.L., 2003. Seasonal cycle of copper speciation in Gullmar Fjord, Sweden. Limnol. Oceanogr. 48, 764–776.
Dyrssen, D., 1988. Sulphide complexation in surface seawater. Mar. Chem. 24, 143–153.
Kadar, E., Powell, J.J., 2006. Post-capture experimental investigations using hydrothermal vent macro-invertebrates to study adaptations to extreme environments. Rev. Environ. Sci. Biotechnol. 5, 193–201.
Kadar, E., Costa, V., Santos, R.S., Powell, J.J., 2005. Enrichment in trace metals Al Mn Co Cu Mo Cd Fe Zn Pb and Hg. of macro-invertebrate habitats at hydrothermal vents along the Mid Atlantic Ridge. Hydrobiology 548, 191–205.
Kennedy, C.B., Scott, S.D., Ferris, F.G., 2004. Hydrothermal phase stabilisation of 2-line ferrihydrite by bacteria. Chem. Geol. 212, 269–277.
Kim, H.H., Mullaugh, K.M., Tsang, J.J., Yucel, M., Luther, G.W., 2008. Formation of Zn- and Fe-sulfides near hydrothermal vents at the Eastern Lau Spreading Center: implications for sulphide bioavailability to chemoautotrophs. Geochem. Trans. 9, 6–74.
Kuma, K., Nishioka, J., Matsunaga, K., 1996. Controls on iron (III) hydroxide solubility in seawater: the influence of pH and natural organic chelators. Limnol. Oceanogr. 41, 396–407.

Lead, J.R., Wilkinson, K.J., Balnoisn, E., Cutak, B.J., Larive, C.K., Assemi, S., Beckett, R., 2000. Diffusion coefficients and polydispersities of the Suwannee River fulvic acid: comparison of fluorescence correlation spectroscopy, pulsed-field gradient nuclear magnetic resonance, and flow field-flow fractionation. Environ. Sci. Technol. 34, 3508–3513.

Lee, C., Kramer, T.A., 2004. Prediction of three-dimensional fractal dimensions using the two-dimensional properties of fractal aggregates. Adv. Colloid Interface Sci. 112, 49–57.

Lin, M.Y., Lindsay, H.M., Weitz, D.A., Ball, R.C., Klein, R., Meakin, P., 1998. Universality of fractal aggregates as probed by light scattering. Nature 339, 360–362.

Long, D.T., Angino, E.E., 1977. Chemical speciation of Cd, Cu, Pb and Zn in mixed freshwater, seawater, and brine solutions. Geochim. Cosmochim. Acta 41, 1183–1191.

Luther, G.W., 2004. In: Wilcock, W.S.D., DeLong, E.F., Kelley, D.S., Baross, J.A., Cary, S.C. (Eds.), AGU Geophysical Monograph 144, The Subsurface Biosphere at Mid-Ocean Ridges. American Geophysical Union, pp. 245–268.

Mavrocordatos, D., Perret, D., Leppard, G., 2007. Characterization of Colloids by Electron Microscopy. Wiley, West Sussex, England.

Morley, N.H., Burton, J.D., Tankere, S.P.C., Martin, J.M., 1997. Distribution and behaviour of some dissolved trace metals in the western Mediterranean Sea. Deep-Sea Res. 44, 675–691.

Özturk, M., Bizsel, N., Steinnes, E., 2003. Iron speciation in eutrophic and oligotrophic Mediterranean coastal waters; impact of phytoplankton and protozoan blooms on iron distribution. Mar. Chem. 81, 19–36.

Perret, D., Gaillard, J.F., Dominik, J., Atteia, O., 2000. The diversity of natural hydrous iron oxides. Environ. Sci. Technol. 34, 3540–3546.

Sander, S.G., Koschinsky, A., 2011. Metal flux from hydrothermal vents increased by organic complexation. Nat. Geosci. 4, 145–150.

Sarthou, G., Jeandel, C., 2001. Seasonal variations of iron concentrations in the Ligurian Sea and iron budge in the Western Mediterranean Sea. Mar. Chem. 74, 115–129.

Spencer-Hall, J.M., Rodolfo-Metalpa, R., Martin, S., Ransome, E., Fine, M., Turner, S.M., Rowley, S.J., Tedesco, D., Buia, M.C., 2008. Volcanic carbon dioxide vents show ecosystem effects of ocean acidification. Nature 454, 96–99.

Stolpe, B., Hassellöv, M., 2010. Nanofibrils and other colloidal biopolymers binding trace elements in coastal seawater: significance for variations in the element size distributions. Limnol. Oceanogr. 55, 187–202.

Toner, B.M., Fakra, S.C., Manganini, S.J., Santelli, C.M., Marcus, M.A., Moffett, J., et al., 2009. Preservation of iron (II) by carbon-rich matrices in a hydrothermal plume. Nat. Geosci. 2, 197–201.

Utsunomiya, S., Ewing, R.C., 2003. Application of high-angle annular dark field scanning transmission electron microscopy (HAADF-STEM), STEM-energy dispersive X-ray spectrometry (EDX), and energy-filtered (EF)-TEM to the characterization of nanoparticles in the environment. Environ. Sci. Technol. 37, 786–791.

Wilkinson, K.J., Juz-Roland, A., Buffle, J., 1997. Different roles of pedogenic fulvic acids and aquagenic biopolymers on colloid aggregation and stability in freshwaters. Limnol. Oceanogr. 43, 1714–1724.

Wilkinson, K.J., Balnois, E., Leppard, G.G., Buffle, J., 1999. Characteristic features of the major components of freshwater colloidal organic matter revealed by transmission electron and atomic force microscopy. Colloids Surf. A-Physicochem. Eng. Asp. 155, 287–310.

Willeke, K., Baron, P.A., 1993. In: Nostrand Reinhold, Van (Ed.), Electrostatic precipitator: Aerosol Measurement: Principles Techniques and Applications, 118, pp. 423–424. Wiley, New York.

Wu, J., Wells, M.L., Remember, R., 2011. Dissolved iron anomaly in the deep tropical-subtropical Pacific: evidence for long-range transport of hydrothermal iron. Geochim. Cosmochim. Acta 75, 460–468.

Yucel, M., Gartman, A., Chan, C.S., Luther, G.W., 2011. Hydrothermal vents as a kinetically stable source of iron-sulphide-bearing nanoparticles to the ocean. Nat. Geosci. 4, 367–371.